PHYSICAL REVIEW B **84**, 115208 (2011)

Organic light-emitting diodes under high currents explored by transient electroluminescence on the nanosecond scale

D. Kasemann,* R. Brückner, H. Fröb, and K. Leo†

Institut für Angewandte Photophysik, George-Bähr-Strasse 1, D-01062 Dresden, Germany

(Received 3 May 2011; revised manuscript received 17 August 2011; published 20 September 2011)

We investigate organic light-emitting diodes (OLEDs) comprising the singlet emitter system 4-dicyanomethylene-2-methyl-6-p-dimethylaminostyryl-4H-pyran (DCM) doped into aluminium tris(8-hydroxyquinoline) (Alq_3) at high excitation densities. With the OLED active area reduced to $100 \times 100\ \mu m^2$, current densities up to 800 A/cm^2 are achieved in pulsed operation. These devices exhibit an intense electroluminescence (EL) turn-on peak on the nanosecond time scale. With the help of streak camera measurements, we prove that the steady state EL of the fluorescent OLEDs is reduced due to singlet-triplet quenching. We demonstrate that short electrical pulses with a rise time of 10 ns make the separation of singlet emission and singlet-triplet quenching in time domain possible. By modeling the singlet and triplet population dynamics in the emission layer, we find that the triplet-triplet annihilation-rate coefficient in doped fluorescent materials is triplet-density dependent at high excitation density. The increased triplet lifetime usually observed in host:guest systems due to triplet trapping on guest molecules vanishes at high current densities. An increase in current density leads to an increased triplet-triplet annihilation rate, while the triplet density in the emission layer stays constant.

DOI: 10.1103/PhysRevB.84.115208 PACS number(s): 78.60.Fi, 81.05.Fb, 85.60.Jb, 71.35.−y

I. INTRODUCTION

Organic solid state lasers (OSLs) have been intensively studied during the last decade due to the beneficial combination of versatile organic materials with the advantages of solid state emitters. The huge amount of available materials exhibiting a broad gain spectrum promise a tunability over the whole visible range, while the solid state character enables a compact device size and the transfer of processing and structuring technology from the inorganic counterpart. Even though various optically pumped devices comprising different resonator types and material combinations have been shown,[1–4] direct electrical pumping has not been achieved yet.[5] The high singlet exciton density needed in the active layer to obtain population inversion is easily created by pulsed optical pumping, but additional losses prevent the excitation to reach the critical point when driven electrically.

Following the presentations of optically pumped OSLs, several groups have reported on organic semiconductors under intense electrical excitation in an attempt to reach the necessary singlet densities. In single layer organic thin films, injection and transport of extremely high current densities up to MA/cm^2 has been achieved.[6–8] Peak brightnesses in the range of 10^6 cd/m^2 were demonstrated at high peak current densities (up to kA/cm^2), both in polymer organic light emitting diodes (OLEDs)[9–12] as well as in small-molecule devices,[13–15] and pulsed excitation was identified as prerequisite for a potential electrically pumped lasing device.[16,17] Singlet quenching due to triplets and polarons is expected to be the main effect restricting laser operation under electrical excitation.[18,19] While the lifetime of a singlet exciton usually is in the range of ns, triplet excitons exhibit a lifetime of μs in phosphorescent materials, and several hundreds of μs up to ms in fluorescent materials. Therefore, the triplet density in an electrically pumped device saturates at several orders of magnitude higher than the singlet density for steady state.

Recently, Gärtner *et al*. investigated the response of an organic double heterostructure laser diode to a current step of 1 kA/cm^2 by numerical simulation.[20,21] They predicted that the effect of triplet absorption on modal gain and thus singlet density can be reduced by a factor of 60 compared to cw operation for a pulse rise time of 5 ns. Hence, a separation of singlets and triplets in the time domain should be possible under electrical excitation. Similar restrictions for an electrically pumped device were reasoned by Giebink *et al*. after investigating the step response of optically pumped OSLs.[22] The optically excited singlet states lead to a reasonable triplet population generated via intersystem crossing. Singlet-triplet quenching then limits the lasing to less than 150 ns following the pump turn on. Therefore, in the case of electrical excitation, short current rise times of less than 50 ns at current densities above 1 kA/cm^2 are required for devices with low cavity losses. Hence, a detailed investigation of the transient turn-on behavior of fluorescent OLEDs under high current densities is expected to give interesting insight into the annihilation processes.

Here, we investigate the behavior of *p-i-n* OLEDs[23] comprising the singlet emitter system 4-dicyanomethylene-2-methyl-6-p-dimethylaminostyryl-4H-pyran (DCM) doped into aluminium tris(8-hydroxyquinoline) (Alq_3) at high excitation densities up to 800 A/cm^2 on the nanosecond time scale. First, we develop a theoretical model incorporating the different loss mechanisms in amorphous organic layers and present the expected behavior of an Alq_3:DCM OLED using a set of literature values in Sec. II. The sample design and measurement setup is explained in Sec. III. After briefly presenting the results of power and time-dependence measurements in Sec. IV, a detailed analysis is given in Sec. V and summarized in Sec. VI.

II. MODELING DEVICE BEHAVIOR

The electrical excitation of organic material leads to the generation of singlet and triplet states. Due to spin statistics these excited states are generated with a ratio of three triplets to one singlet.[24] OLEDs benefit from this ratio by the incorporation of phosphorescent emitting materials. In these organic materials a radiative transition from the first

excited triplet state to the lowest singlet state is enabled by spin-orbit coupling, hence the internal quantum efficiency approaches unity. Unfortunately these devices suffer from a huge efficiency roll off at the high excitation densities resulting from the long triplet lifetimes.

The interaction of two triplet excitons (T_1) leads to an energy transfer from the first to the second exciton which is excited to a higher-lying state that subsequently relaxes either to the first-excited singlet or triplet state. The ratio of singlet and triplet excitons generated by this process is determined by spin statistics (1/4 singlets, 3/4 triplets). This process is known as triplet-triplet annihilation (TTA) with the rate coefficient κ_{TT} and can be written as

$$T_1 + T_1 \xrightarrow{3/4\ \kappa_{TT}} T_1 + S_0, \tag{1}$$

$$T_1 + T_1 \xrightarrow{1/4\ \kappa_{TT}} S_1 + S_0. \tag{2}$$

Triplet-polaron annihilation (TPA) is the interaction of excited triplet excitons with electrons and holes and is given by

$$T_1 + n \xrightarrow{\kappa_{TP}} S_0 + n, \tag{3}$$

with κ_{TP} as the rate coefficient. Unfortunately, up to now only singlet-emitter systems have been proven to exhibit lasing, thus restricting the material choice to fluorescent emitters. In these materials a huge population of optically inactive and long-lived excited triplet excitons is built up during operation. This leads to quenching of singlet excitons and an efficiency roll off at high excitation densities by singlet-triplet annihilation (STA):

$$S_1 + T_1 \xrightarrow{\kappa_{ST}} T_1 + S_0, \tag{4}$$

with the corresponding rate coefficient κ_{ST}. The singlet exciton population is also reduced by the singlet-singlet annihilation (SSA) with the rate coefficient κ_{SS}:

$$S_1 + S_1 \xrightarrow{\kappa_{SS}} S_1 + S_0. \tag{5}$$

Here, a change in spin symmetry is not possible by nonradiative energy transfer, therefore only singlet excitons result from SSA. Furthermore, singlet excitons can be quenched by electrons and holes, characterized by κ_{SP}, which is the rate coefficient for singlet-polaron annihilation (SPA):

$$S_1 + n \xrightarrow{\kappa_{SP}} S_0 + n. \tag{6}$$

Finally, excited singlet excitons can undergo intersystem crossing (ISC). In this process the singlet exciton is transferred to an excited triplet exciton by the help of spin-orbit coupling. The corresponding rate coefficient is κ_{ISC}:

$$S_1 \xrightarrow{\kappa_{ISC}} T_1. \tag{7}$$

By accounting for these annihilation processes, the dynamics of excited states in OLEDs can be characterized by the following set of rate equations:[20,25] Assuming Langevin recombination and balanced charges ($n = p$), the polaron population n is given by

$$\frac{dn}{dt} = \frac{J(t)}{ed} - \gamma n^2, \tag{8}$$

with the current density $J(t)$ at time t and the width of the recombination zone d. This description for the polaron generation given in [25] neglects the charge transit times within the device. With ϵ_0 as the permittivity of free space and the relative permittivity of the emission layer $\epsilon_r = 2.9$, the Langevin recombination rate[26] γ can be written as

$$\gamma = \frac{e\,(\mu_e + \mu_h)}{\epsilon_0 \epsilon_r}. \tag{9}$$

Here, μ_e and μ_h are the mobilities of electrons and holes in the emission layer, respectively. Taking into account the processes affecting the excited singlet states [Eqs. (2) and (4)–(7)], their population can be described by the following equation:

$$\frac{dS_1}{dt} = \frac{1}{4}\gamma n^2 - \kappa_S S_1 - \kappa_{SS} S_1^2 - \kappa_{ST} S_1 T_1 + \frac{1}{4}\kappa_{TT} T_1^2 - 2\kappa_{SP} n S_1 - \kappa_{ISC} S_1. \tag{10}$$

Here, κ_S denotes the radiative and nonradiative decay of singlet excitons. The prefactors arise from spin statistics and the amount of excited singlets lost or gained per process.[20] With κ_T being the triplet decay rate, the triplet population is given by

$$\frac{dT_1}{dt} = \frac{3}{4}\gamma n^2 - \kappa_T T_1 - \frac{5}{4}\kappa_{TT} T_1^2 - 2\kappa_{TP} n T_1 + \kappa_{ISC} S_1. \tag{11}$$

Field-assisted dissociation of excitons is omitted in the description given above. Although field quenching is expected to reduce the absolute exciton densities by a few percent at applied fields above 2 MV/cm, the effect on the dynamics of singlet and triplet population is neglected.[27–29] This set of coupled nonlinear rate equations allows us to model the device behavior after turn on. Figure 1(a) shows the singlet and triplet population dynamics for 40 nm Alq_3 doped with 2 wt% DCM, the corresponding rate coefficients are summarized in Table I.

As the electron mobility in Alq_3 is one order of magnitude larger than the hole mobility, the exciton formation region is assumed to be close to the hole injection side. Hence, the hole mobility is neglected in Eq. (9). The dynamics are calculated for a current density of 1 kA/cm^2 and a mobility of $\mu_e = 1 \times 10^{-5}$ cm^2 V^{-1} s^{-1} [Fig. 1(a)], as given in the literature.[32] After the set in of the current at $t = 0$ the polaron population quickly rises and saturates after 25 ns. Excited singlet and triplet excitons are generated with the ratio of 1 to 3. At low density, the singlet population is mainly determined by the decay rate κ_S. As the triplet density rises, STA starts to dominate and thus limits the singlet population to its steady state value. The "overshoot" in the singlet population indicates that it is possible to reach high singlet densities even in materials suffering from high STA by separating the different effects in time. We can increase this effect and compress it in time by accounting for a field-dependent mobility. Because very high fields have to be applied to the emission layer to achieve the desired current densities, an increased mobility is reasonable. A higher mobility directly translates into a faster exciton generation by the Langevin recombination rate γ. Assuming an electron mobility of 2×10^{-4} cm^2 V^{-1} s^{-1} in the emission layer, the peak singlet density rises from 2.6×10^{16} to 8.7×10^{16} cm^{-3} [Fig. 1(b)]. However, these calculations end up in an unrealistically high triplet density which saturates

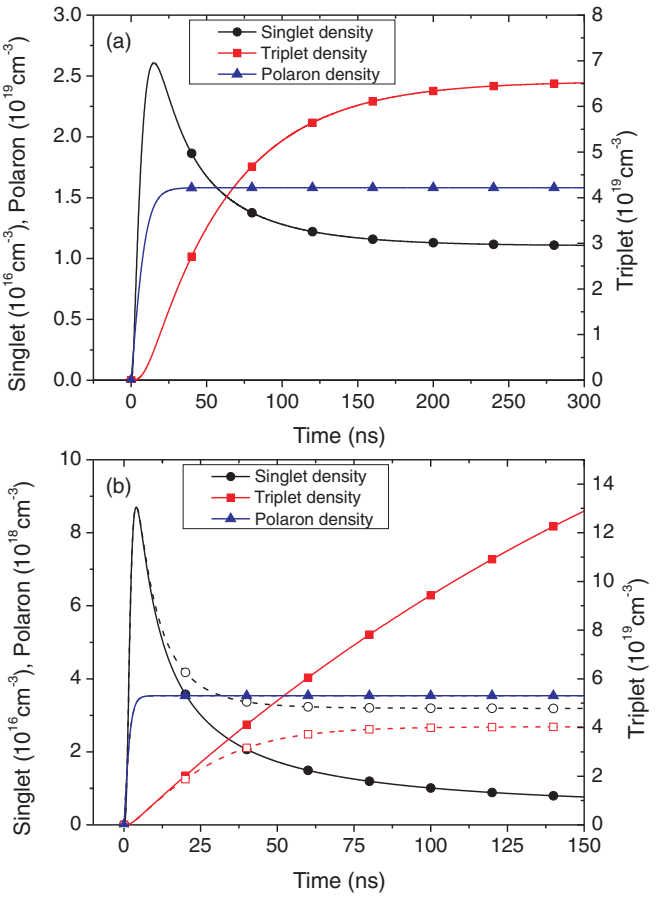

FIG. 1. (Color online) Singlet and triplet population dynamics for 40 nm Alq_3 doped with 2 wt% of DCM at a current density of 1 kA/cm^2 (rate coefficients are summarized in Table I). (a) The electron mobility in the emission layer is set to $\mu_e = 1 \times 10^{-5}$ cm^2 V^{-1} s^{-1}, as given in the literature. (b) An increased mobility of $\mu_e = 2 \times 10^{-4}$ cm^2 V^{-1} s^{-1} due to the increased applied field is assumed. The closed symbols indicate the dynamics for the low κ_{TT} of the host:guest system. The open symbols (dashed lines) have been calculated with a TTA rate of $\kappa_{TT} = 5.0 \times 10^{-13}$ cm^3/s, a value much closer to the one for pristine Alq_3.

at a value of $T_1 = 3.4 \times 10^{20}$ cm^{-3} after 1 ms. An amorphous layer of Alq_3:DCM consists of only 1.7×10^{21} molecules per cm^3. Hence, this would imply that every fifth molecule is in the first-excited triplet state. To justify that this is unrealistically high, we discuss the origin of the low TTA rate in the emission layer (EML) in the following paragraph.

Fluorescent host:guest systems suffer from an increased triplet lifetime due to a reduced TTA rate. Under electrical excitation, this leads to the accumulation of a huge triplet density affecting the singlet density as seen above. Lehnhardt *et al.*[31] recently demonstrated this effect for Alq_3:DCM; the values for the rate coefficients are listed in Table I. A pristine Alq_3 layer exhibits a three orders of magnitude higher TTA rate compared to a layer doped with 2 wt% of DCM. This effect is explained by a reduced triplet diffusion in the doped layer due to the guest molecules acting as triplet traps. The reduced triplet diffusion directly relates to the TTA rate because it reduces the probability that two triplets meet. These measurements have been performed at triplet densities on the order of 1×10^{17} cm^{-3}, three orders of magnitude lower than the density of DCM guest molecules.

TABLE I. Literature values for the system Alq_3:DCM. The value for κ_{SP} is given for CBP:DCM. Additionally, κ_{TT} for pristine Alq_3 is listed.

Coefficient	Value	Reference
κ_S	1.0×10^{9} s^{-1}	25
κ_{SS}	3.5×10^{-12} cm^3/s	30
κ_{ST}	1.9×10^{-10} cm^3/s	25, 22
κ_{ISC}[a]	1.5×10^{8} s^{-1}	22
κ_T[b]	6.5×10^{2} s^{-1}	31
κ_{TT}	2.2×10^{-15} cm^3/s	25, 31
κ_{TP}	2.8×10^{-13} cm^3/s	25
κ_{SP} (CBP:DCM)	3.0×10^{-10} cm^3/s	19
κ_{TT} (Alq_3)	2.2×10^{-12} cm^3/s	31

[a] $\kappa_{ISC} = \Phi_T/\tau_S$, $\Phi_T = 0.15$.
[b] $\kappa_T = 1/\tau_T$, $\tau_T = 1.55$ ms.

Our calculations in Fig. 1(b) result in a triplet density one order of magnitude higher than the DCM density. In this excitation regime the triplet diffusion can no longer limit the TTA rate. Thus, it is reasonable to assume a value for κ_{TT} closer to the one for pristine Alq_3. A justified steady state triplet density should therefore be close to the guest-molecule density. Additional triplet states created on the host molecules are expected to be mobile and undergo TTA at a higher rate. As an example, the open symbols in Fig. 1(b) have been calculated for $\kappa_{TT} = 5.0 \times 10^{-13}$ cm^3/s, a value still one order of magnitude below that of Alq_3. In this case, the triplet density saturates at 4×10^{19} cm^{-3}, resulting in every 42nd molecule being in an excited triplet state. As this is still slightly more than the amount of available DCM molecules, the triplets cannot be completely trapped on guest molecules.

III. SAMPLE PREPARATION AND MEASUREMENTS

In this paper, we investigate OLEDs having a standard *p-i-n*[23] structure incorporating *p*- and *n*-doped transport layers, intrinsic exciton-blocking layers, and a host:guest system as active layer. The devices are built on patterned indium-tin-oxide- (ITO) coated glass substrates with a bottom contact of 100 μm width. After cleaning the substrates in an ultrasonic bath (acetone, ethanol, and isopropanol) followed by an oxygen plasma treatment, the organic material is deposited via thermal evaporation under high-vacuum conditions (base pressure of 10^{-8} mbar) in a cluster tool. The samples consist of 50 nm N,N'-diphenyl-N,N'-bis(3-methylphenyl)-[1,1′-biphenyl]-4,4′-diamine (MeO-TPD) doped with 2,2′-(perfluoronaphthalene-2,6-diylidene)dimalononitrile (F6TCNNQ) and 50 nm Cs-doped 4,7-diphenyl-1,10-phenanthroline (BPhen) as transport layers. 10 nm N,N'-di(naphthalen-1-yl)-N,N'-diphenyl-benzidine (αNPD) and 10 nm intrinsic BPhen serve as electron- and hole-blocking layers (EBL, HBL), respectively. As emission layer (EML), 2 wt% of the fluorescent emitter 4-dicyanomethylene-2-methyl-6-p-dimethylaminostyryl-4H-pyran (DCM) are doped into 40 nm aluminium tris(8-hydroxyquinoline) (Alq_3). Finally, a 100 nm Al cathode is structured by shadow-mask evaporation, defining

an active area of 100 × 100 μm^2. The film thicknesses and doping ratios are controlled with the help of independent quartz crystal monitors. The organic layers are deposited without breaking the vacuum. A transfer to a nitrogen glove box is necessary to position the shadow mask for the Al evaporation. We encapsulate the samples with epoxy glue and glass lids under nitrogen atmosphere prior to measurement.

As the active area of the devices is very small, a microscope setup is used to carry out the measurements. The emitted light is collected using an objective with a numerical aperture of 0.65 (20× magnification) and focused onto an exchangeable detector. Emission spectra are recorded using an Ocean Optics visible–near-infrared spectrometer (USB4000), while the time-dependent signal is measured by a fast Si photo diode (ThorLabs PDA10A). The data acquisition is carried out on a digital oscilloscope (HP 54815A). The voltage is measured directly across the sample and corrected for the series resistance of the supply lines. The current signal is derived from an additional pulse-withstanding series resistor. The streak camera measurements are conducted using a combination of C5680 and M5677 by Hamamatsu Photonics (temporal resolution better than 50 ps, sweep time up to 1 ms) and a blue diode laser (Coherent Cube 405 nm, 50 mW) is used as source for the optical excitation. The electrical excitation is done either with a high-power pulse generator (HP 8114A) or with a fast home-built switch with a rise time of 10 ns.

IV. RESULTS

After preparation and encapsulation under nitrogen atmosphere, the samples are measured in pulsed-mode operation. The excitation is done with 50 ns pulses at a repetition rate of 1 kHz, resulting in a duty cycle of 5 × 10^{-5}. The low duty cycle makes measurements at high current densities possible without the need of additional cooling. This can be shown by investigating a single *p*-doped transport layer (100 nm MeO-TPD doped by 4 wt% 2,3,5,6-Tetrafluoro-7,7,8,8-tetracyanoquinodimethane, F4-TCNQ) sandwiched between two metal electrodes (Fig. 2). While the maximum current density is limited to 230 A/cm^2 at 5 μs pulses (500 Hz), an identical sample sustains up to 6.2 kA/cm^2 at 50 ns pulses (1 kHz).

A. Power-dependent electroluminescence

To explore the maximum possible current densities, the *J*-*U* characteristic of a *p*-*i*-*n* OLED comprising 40 nm Alq_3 doped by 2 wt% DCM is measured up to destruction while simultaneously evaluating the emission spectra (Fig. 3). Each data point in the *J*-*U* curve is recorded 5000 times; the current and voltage curves are averaged over 1024 measurements at the oscilloscope. The maximum current density of 800 A/cm^2 is limited by a catastrophic device failure. The organic layers crystallize and the Al top contact is destroyed, ending up in an open contact. Nevertheless the device is very stable for current densities below this maximum. For example, the sample can be operated at a 500 A/cm^2 for several hours with no sign of degradation in current and voltage curves or in emission. The OLED shows the expected emission

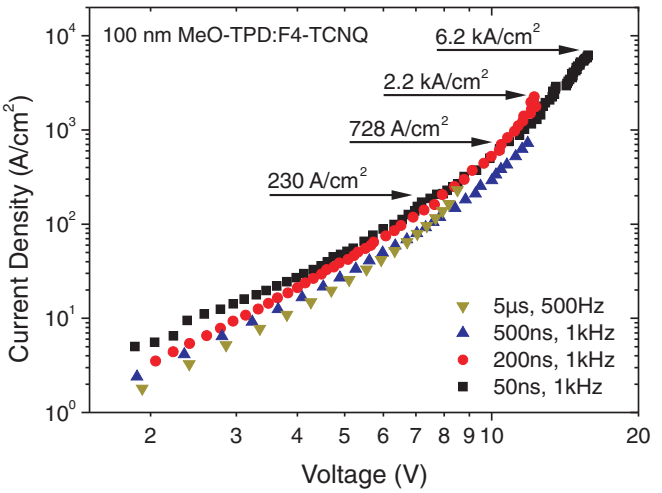

FIG. 2. (Color online) A 100 nm *p*-transport layer (MeO-TPD doped by 4 wt% F4-TCNQ) between two metal electrodes excited at different pulse lengths and duty cycles.

around 610 nm and exhibits no significant wavelength shift. The integrated area under the emission spectrum [Fig. 3(c)] nicely demonstrates that the emission intensity continuously increases with increasing input power.

B. Time-resolved electroluminescence

The time-resolved EL data and corresponding fitting curves are plotted in Fig. 4(a). A rectangular voltage pulse with a width of 100 ns and a rise time of 10 ns is applied to the OLED. The current, voltage, and photo diode signal is averaged over 256 pulses and corrected for the diode dark current. The singlet-emitter system shows a very fast turn-on and turn-off of the device due to the short DCM singlet lifetime of about

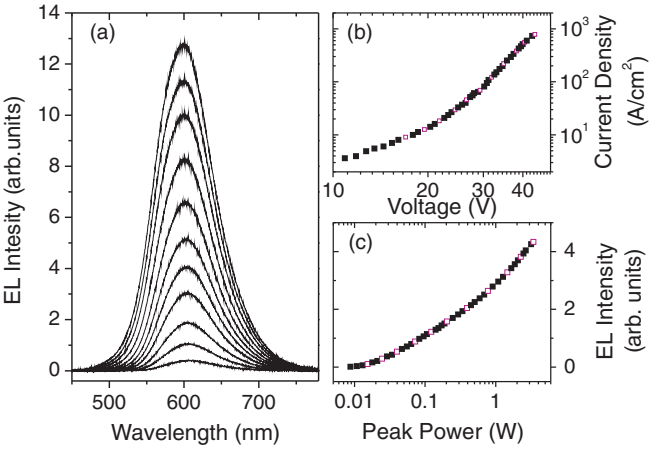

FIG. 3. (Color online) (a) Emission spectra of an Alq_3:DCM (2 wt%) OLED under pulsed excitation at different current densities (50 ns pulses, 1 kHz repetition rate). The *J*-*U* characteristic is given in (b), and the integrated area under the spectrum is plotted vs the input power in (c). A reduced amount of emission spectra is depicted here; the corresponding points in the *J*-*U* characteristics are indicated by the open red symbols. The emission intensity continuously increases with current density up to 800 A/cm^2 and shows no shift in emission wavelength.

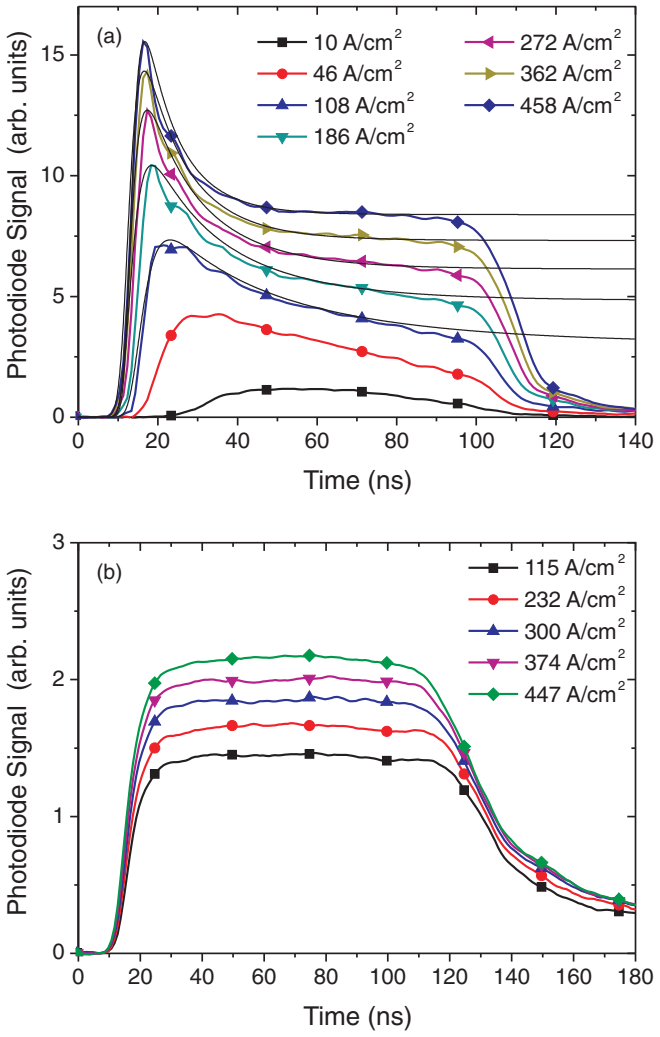

FIG. 4. (Color online) (a) Time-resolved EL signal of an Alq_3:DCM (2 wt%) OLED in response to a 100 ns rectangular voltage pulse at different current densities. The thin black lines indicate the calculated behavior. (b) Time-resolved EL signal of an OLED with undoped Alq_3 EML at similar current densities and slightly longer pulses for comparison. Details are given in Sec. V.

1 ns.[25] The turn-on delay ranges from 20 ns for 10 A/cm^2 down to 5 ns for the highest current densities. The amplitude of the EL-turn-on overshoot increases with current density while its width decreases. At a current density of 458 A/cm^2 a steady state EL is reached after only 60 ns. The lowest current density is limited by the sensitivity of the setup. Additionally, the time-resolved EL signal of an OLED based on the same layer stack, but equipped with an undoped Alq_3 EML, is shown in Fig. 4(b) for comparison. The undoped OLED features the same fast turn on and turn off; however, an EL overshoot is not observed in this case.

C. Proof of singlet quenching

By using a combination of electrical excitation and optical probe, the following streak camera measurements directly show that the reduced steady state EL of the DCM-doped OLED is caused by singlet quenching. One might argue that the EL overshoot shown in the time-resolved measurements originates from electrical device properties. Therefore, we use the blue diode laser focused to the electrically active device area to optically excite singlet states in the EML. By comparing the DCM photoluminescence (PL) before and after an electrical pulse, we directly probe the singlet quenching. The results of the streak camera experiments are summarized in Fig. 5. First, a 280 ns laser pulse gives the PL intensity in the absence of triplet states (the tail appears in the streak camera images). After a short delay, a 150 ns voltage pulse with different amplitudes is applied to the sample [Figs. 5(a)–5(c)]. This pulse leads to EL and the occupation of triplet states. Finally, a second laser pulse (280 ns) again generates only singlet states in the EML. Line cuts of the first and second PL pulse are plotted in Fig. 5(d) (normalized to the intensity of the first pulse). These measurements are performed at a repetition rate of 1 kHz. The PL intensity within this second optical pulse decreases with increasing EL intensity. This directly proves that singlet annihilation is the cause for the reduced steady state intensity.

D. Quenching states lifetime

Using a double pulse with varying delay, we can prove that the reduced steady state EL is caused by long-lived quenching states. While the first voltage pulse fills the quenching states, the turn-on behavior of the second pulse probes their residual occupation. A double pulse with a width of 50 ns at a current density of 490 A/cm^2 is applied to the sample (repetition rate 100 Hz). Figure 6 depicts the EL signal for the second pulse at a varied double-pulse delay. The EL-turn-on overshoot vanishes for a delay less than 10 μs and gradually recovers with increasing delay. The values for the intensity of the turn-on overshoot of the second pulse are recorded for different double-pulse delay and normalized to the intensity of the overshoot of the first pulse. After subtracting the intensity of the first pulse overshoot, these values are plotted vs the double-pulse delay time (unity-normalized overshoot vs delay; see inset of Fig. 6). A recovery time of more than 1 ms is necessary for the EL to reach its initial turn-on value.

To exclude that trapped charges and the resulting field distribution across the sample cause the EL overshoot or the singlet quenching after electrical excitation, the time-resolved experiments are repeated with an additional electric field applied to withdraw trapped charges from the device. For this purpose, a negative bias voltage resulting in a field of up to 1.4 MV/cm is applied to the sample between the pulses. With increasing negative field, the EL turn-on delay increases. This is the case for a single pulse as given in Sec. IV B, as well as for the second pulse in the double-pulse experiments. The shape of the transient EL signals, however, does not change. The increased turn-on delay can be explained by an enlarged depletion layer in the device center, resulting in an increased charge transit time after the onset of the current. As the recovery time of the EL overshoot does not change with the additional field, a significant contribution of space charges to the singlet exciton quenching observed in streak camera measurements can be excluded.

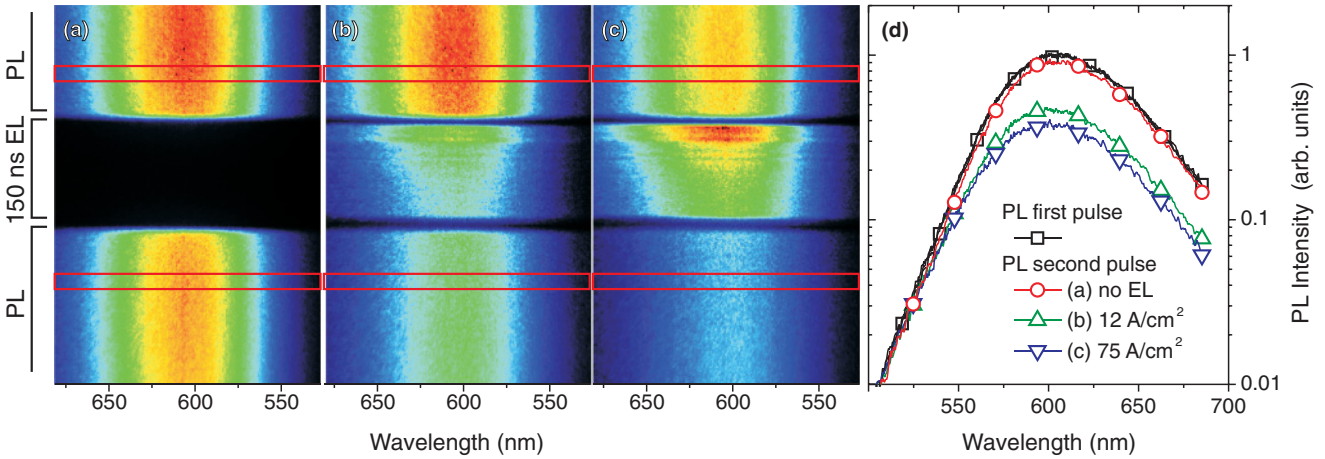

FIG. 5. (Color online) Streak camera measurements combining electrical excitation (150 ns pulses) with an optical probe. The current density within the EL pulse is varied [(a) no EL, (b) 12 A/cm^2, (c) 75 A/cm^2] while the optical-pump intensity is kept constant. The plot (d) shows line cuts at the times indicated by the red boxes in (a)–(c). The PL intensity is significantly reduced after an electrical excitation.

V. DISCUSSION

One of the main factors limiting the current density in organic devices at high excitation density is the Joule heat generated in the organic layers. The variation of the duty cycles and pulse lengths in the single *p*-doped transport layer nicely demonstrates this fact. Keeping the excitation pulses short, the duty cycle low, and the active area small reduces the energy to be dissipated from the sample, thus enabling higher current densities. Similar indications for the duty cycle have been given by Tessler *et al.*[33] investigating the current-induced heating in a single-layer polymer light-emitting diode. Another way of increasing the maximum current density is the use of substrates with higher thermal conductivity,[6,8,14] once again indicating a clear relationship between the maximum current density and the Joule heat generated in the organic layers.

The *J*-*U* characteristics in Fig. 3 show that our device sustains current densities up to 800 A/cm^2 for the chosen excitation scheme. Even though the applied voltage of 40 V is one order of magnitude larger than the band gap of the organic materials, the spectra indicate that the emission originates from the DCM molecules. An increased emission from other layers within the device would result in an additional peak in the emission spectrum. This has not been observed within the visible spectral range.

The time-resolved measurements in Fig. 4 give us an insight into the singlet and triplet dynamics at turn on. The Alq_3:DCM OLED exhibits a strong EL-turn-on overshoot at high current densities, similar to the characteristics predicted by Eqs. (8)–(11). As the emission originates from the DCM singlets, its intensity relates to the singlet density within the EML. While the overshoot increases and narrows with increasing current density, the time to reach steady state decreases. The time-resolved measurements of an undoped Alq_3 OLED shown in Fig. 4(b), however, do not exhibit an EL overshoot. By comparing these two samples, the effect of field-induced exciton dissociation can be ruled out as a cause for the turn-on overshoot. One might argue that the rise time of the voltage pulse leads to a slowly increasing electric field across the EML, enabling a higher emission intensity due to reduced field quenching in the beginning of the optical pulse. However, if the rise time of the voltage pulse was the cause for the EL overshoot, then the same effect should be observed for the undoped Alq_3 OLED. The overshoot in the undoped OLED should be even stronger, as field quenching is less effective for DCM doped into Alq_3, compared to pure Alq_3.[27] The behavior of the undoped Alq_3 OLED therefore proves that field quenching does not effect the dynamics of the EL on the time scale observed. Furthermore, although the both devices exhibit the same electrical properties, the overshoot is only observed in the device with the doped EML. Consequently, the EL overshoot is not caused by the transient shape of the space-charge-limited currents.

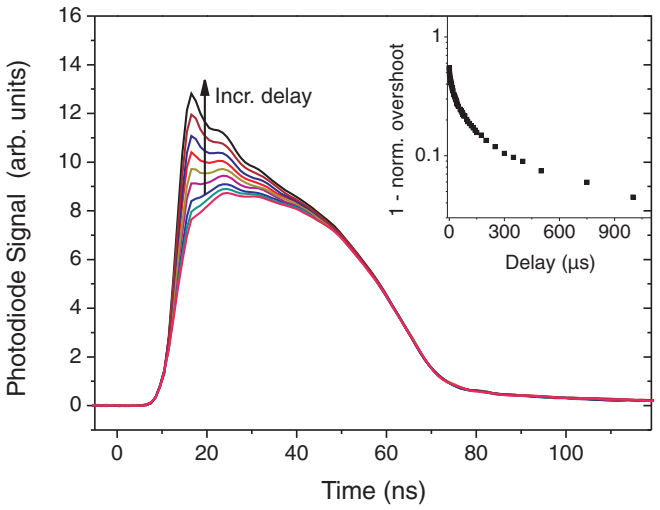

FIG. 6. (Color online) A double pulse with a width of 50 ns and varying double-pulse delay is applied to the sample (J = 490 A/cm^2). The EL signal of the second pulse is depicted here. The turn-on overshoot probes the residual triplet population and increases with increasing delay. The inset gives a plot of unity-normalized intensity of the EL-turn-on overshoot of the second pulse (normalized to the overshoot intensity of the first pulse) vs the double-pulse delay.

The streak camera measurements in Sec. IV C directly prove that the reduced steady state EL is caused by singlet exciton quenching. According to the double-pulse experiments, the quenching states exhibit a lifetime of around 1 ms, which is the expected lifetime of triplet states in Alq_3:DCM (Table I). Furthermore, trapped charges can be excluded as quenching states according to the time-resolved measurements with negative bias. Moreover, STA as cause for the EL overshoot in the DCM-doped device also explains the absence of an overshoot in the undoped device. Because STA takes place via long-range Förster energy transfer, its rate coefficient depends on the spectral overlap of the fluorescence of the donor with the triplet-triplet absorption band of the acceptor molecule. In thin films, Alq_3 exhibits a triplet absorption maximum around 600 nm with an additional shoulder at 700 nm.[34] In a pure Alq_3 OLED therefore, the spectral overlap of the singlet emission around 540 nm with the triplet absorption is small. Hence, STA is inefficient and an EL overshoot due to STA is not observed. In the Alq_3:DCM device, however, the singlet emission of the DCM molecules at 610 nm exhibits a strong overlap with the Alq_3 triplet absorption. The Alq_3 triplet excitons therefore lead to an efficient nonradiative depopulation of the DCM singlet excitons in the doped OLED, resulting in the observed EL-turn-on overshoot. Hence, the quenching state decay depicted in Fig. 6 directly relates to the triplet exciton decay in the EML. Nevertheless, a simple fit of the decay using TTA is not possible due to the expected density dependence of κ_{TT} at the excitation densities used here (see Sec. II). If the EL overshoot in the DCM-doped devices originates from STA, we should be able to fit the time-resolved measurement with the model given in Sec. II.

The charge carrier mobility can be extracted from the turn-on delay of the sample at different applied voltages. We assume no voltage drop across the electrically doped layers; thus, the complete field is applied across the inner layers (10 nm EBL)/(40 nm EML)/(10 nm HBL). This assumption is valid for low current densities while it leads to an underestimation of the mobility for the case of a voltage drop across the transport layers. Hence, the extracted value will be a lower limit for the mobility. The electron mobility in the EML is higher than the hole mobility, leading to a recombination zone at the EBL-EML interface. Therefore, we determine an average mobility for HBL and EML. From the measurements in Fig. 4(a), we extract an electron mobility of $(2 \pm 1) \times 10^{-4}$ cm^2 V^{-1} s^{-1} at a field 7.3 MV/cm. This value is reasonable assuming a Poole-Frenkel–type field dependence of the mobility.

The equations in Sec. II assume an onset of the current at $t = 0$, omitting the pulse rise time. In our measurements, however, we are limited to a minimal voltage rise time of 10 ns. This also affects the current rise time and overlays the EL-turn-on overshoot. Therefore, we include the rise time in the set of equations by a time-dependent current density. We model the measured current by the following function:

$$J(t) = J_{\max} - \frac{J_{\max}}{1 + e^{(t-t_0)/dt}}. \tag{12}$$

Here, $J_{\max}$ is the final current density and the parameters t_0 and dt determine its rise time. The charge transit time is omitted as we assume that the pulse shape is not significantly changed.

TABLE II. Fit parameters and the resulting steady state triplet density at different current densities assuming an electron mobility of 3×10^{-4} cm^2 V^{-1} s^{-1}.

Current Density [A/cm^2]	κ_{TT} [$\times 10^{-13}$ cm^3/s]	T_1 [$\times 10^{19}$ cm^{-3}]
108	3.0	1.6
186	5.5	1.7
272	7.3	1.8
362	9.1	1.8
458	11.9	1.8

The charge transit should only lead to a turn-on delay. This extended set of equations now enables us to fit the experimental data.

For a consistent fit, the electron mobility is set to 3×10^{-4} cm^2 V^{-1} s^{-1}, which is within the range derived from the turn-on delay. Only the TTA rate coefficient is used as a fit parameter, as is expected to become density dependent at these high excitation rates (see Sec. II). The remaining rate coefficients are assumed to be density and field independent and are kept at the literature values (Table I). The resulting fit curves are indicated by the thin black lines in Fig. 4(a); the fit parameters are summarized Table II. The TTA rate increases with increasing current density up to a value close to that of pristine Alq_3. The triplet density saturates at a value corresponding to every 100th molecule within the emission layer in an excited triplet state. This confirms our expectation that the TTA rate in host:guest systems is triplet-density dependent. At high excitation densities the trapping of triplets on guest molecules no longer limits the TTA. A sufficient amount of mobile triplets leads to an increased TTA rate with an increasing exciton-generation rate. Furthermore the TTA is the dominating effect defining the steady state triplet density and, thereby, the singlet steady state value at high excitation densities. At 458 A/cm^2 the polaron density saturates at a value of 2.0×10^{18} cm^{-3}. Thus, the TTA term in Eq. (11) that is proportional to the square of the triplet density ($\propto T_1^2$) is at least ten times larger than the one for TPA ($\propto n T_1$). The measurement data for the two lowest current densities could not be fit because the steady state is not reached within the first 100 ns. To successfully fit the data, the ratio of EL-turn-on overshoot to steady state intensity is needed. These results prove that it is indeed possible to separate singlet emission and singlet-triplet quenching in the time domain.

Although the density dependence of κ_{TT} is indisputable, the absolute numbers for the TTA rate coefficient and the saturation triplet density have to be treated with caution. The reason is that the value of the SPA rate coefficient used to fit the measurement had to be taken from the material combination 4,4′-*N*,*N*′-dicarbazole-biphenyl (CBP) doped by DCM due to the lack of a value for the system Alq_3:DCM. In both systems, the polaron is assumed to be located on the DCM guest molecule due the lower band gap. Furthermore, the singlet is also expected to be located on DCM due to Förster resonance energy transfer from Alq_3. Therefore, the two systems should exhibit similar SPA rate coefficients. However, the host materials could lead to a different dielectric surrounding of the guest molecules, justifying a different κ_{SP}.

Consequently, we performed a variation of κ_{SP} to evaluate its effect on the values given above. At a value of 3.0×10^{-10} cm^3/s, SPA has a non-negligible effect on the singlet and triplet population. A slightly increased SPA rate of 4.5×10^{-13} cm^3/s results in a broadening of the singlet peak which is not explicable using reasonable values for the charge carrier mobility. A lower SPA rate coefficient, however, can be justified with the present data. The singlet peak is narrowed with decreasing SPA while the absolute triplet and singlet densities slightly increase. Neglecting the SPA still leads to a successful fit of the experimental data. The resulting TTA rate for the highest current density is 2.0×10^{-12} cm^3/s while the triplet density saturates at 1.4×10^{19} cm^{-3}.

VI. SUMMARY

In summary, we demonstrate that OLEDs sustain very high current densities in pulsed operation. An Alq_3:DCM OLED exhibits a continuous increase of the EL intensity from the DCM molecules with increasing current density up to 800 A/cm^2. Short electrical pulses with a rise time of only 10 ns allow for the separation of singlet emission and singlet-triplet quenching in the time domain in fluorescent devices. With the help of streak camera measurements, we prove that the reduced steady state EL of fluorescent OLEDs at high current densities results from singlet-triplet quenching. Finally, we indicate that the triplet-triplet annihilation-rate coefficient in doped fluorescent materials is triplet-density dependent at high excitation density. The recently reported increased triplet lifetime in host:guest systems due to triplet trapping on guest molecules vanishes at high current densities. An increase in current density leads to an increased triplet-triplet annihilation rate while the triplet density in the emission layer stays constant. We believe that these results are of significant importance for the field of OSL research as we demonstrate that high singlet exciton densities can be reached in organic materials by electrical excitation.

ACKNOWLEDGMENTS

The authors thank Ralf Raupach and Hans Kleemann for several helpful discussions. This work was financially supported by the German Federal Ministry for Education and Research (BMBF, FKZ 13N9279) and the German Research Foundation (DFG, LE 747/37-1, LE 747/41-1).

*Daniel.Kasemann@iapp.de
†http://www.iapp.de

[1] V. G. Kozlov, V. Bulović, P. E. Burrows, and S. R. Forrest, Nature (London) **389**, 362 (1997).
[2] V. Bulović, V. G. Kozlov, V. B. Khalfin, and S. R. Forrest, Science **279**, 553 (1998).
[3] M. Koschorreck, R. Gehlhaar, V. G. Lyssenko, M. Swoboda, M. Hoffmann, and K. Leo, Appl. Phys. Lett. **87**, 181108 (2005).
[4] I. D. W. Samuel and G. A. Turnbull, Chem. Rev. **107**, 1272 (2007).
[5] I. D. W. Samuel, E. B. Namdas, and G. A. Turnbull, Nat. Photonics **3**, 546 (2009).
[6] W. Yokoyama, H. Sasabe, and C. Adachi, Jpn. J. Appl. Phys. **42**, L1353 (2003).
[7] T. Matsushima, H. Sasabe, and C. Adachi, Appl. Phys. Lett. **88**, 033508 (2006).
[8] H. Yamamoto, H. Kasajima, W. Yokoyama, H. Sasabe, and C. Adachi, Appl. Phys. Lett. **86**, 083502 (2005).
[9] N. Tessler, N. T. Harrison, and R. H. Friend, Adv. Mater. **10**, 64 (1998).
[10] D. J. Pinner, R. H. Friend, and N. Tessler, J. Appl. Phys. **86**, 5116 (1999).
[11] V. Savvateev, A. Yakimov, and D. Davidov, Adv. Mater. **11**, 519 (1999).
[12] I. H. Campbell, D. L. Smith, C. J. Neef, and J. P. Ferraris, Appl. Phys. Lett. **75**, 841 (1999).
[13] B. Wei, M. Ichikawa, K. Furukawa, T. Koyama, and Y. Taniguchi, J. Appl. Phys. **98**, 044506 (2005).
[14] H. Nakanotani, T. Oyamada, Y. Kawamura, H. Sasabe, and C. Adachi, Jpn. J. Appl. Phys. **44**, 3659 (2005).
[15] H. Nakanotani, H. Sasabe, and C. Adachi, Appl. Phys. Lett. **86**, 213506 (2005).
[16] N. Tessler, Adv. Mater. **11**, 363 (1999).
[17] N. Tessler, D. J. Pinner, V. Cleave, D. S. Thomas, G. Yahioglu, P. Le Barny, and R. H. Friend, Appl. Phys. Lett. **74**, 2764 (1999).
[18] V. G. Kozlov, G. Parthasarathy, P. E. Burrows, V. B. Khalfin, J. Wang, S. Y. Chou, and S. R. Forrest, IEEE J. Quantum. Electron. **36**, 18 (2000).
[19] M. A. Baldo, R. J. Holmes, and S. R. Forrest, Phys. Rev. B **66**, 035321 (2002).
[20] C. Gärtner, C. Karnutsch, U. Lemmer, and C. Pflumm, J. Appl. Phys. **101**, 023107 (2007).
[21] C. Gärtner, *Organic Laser Diodes—Modelling and Simulation* (Universitätsverlag Karlsruhe, Karlsruhe, 2009), ISBN 978-3-86644-345-7.
[22] N. C. Giebink and S. R. Forrest, Phys. Rev. B **79**, 073302 (2009).
[23] K. Walzer, B. Maennig, M. Pfeiffer, and K. Leo, Chem. Rev. **107**, 1233 (2007).
[24] M. A. Baldo, D. F. O'Brien, M. E. Thompson, and S. R. Forrest, Phys. Rev. B **60**, 14422 (1999).
[25] Y. Zhang, M. Whited, M. E. Thompson, and S. R. Forrest, Chem. Phys. Lett. **495**, 161 (2010).
[26] B. Ruhstaller, S. A. Carter, S. Barth, H. Riel, W. Riess, and J. C. Scott, J. Appl. Phys. **89**, 4575 (2001).
[27] Y. Luo, H. Aziz, Z. D. Popovic, and G. Xu, Appl. Phys. Lett. **89**, 103505 (2006).
[28] S. Reineke, K. Walzer, and K. Leo, Phys. Rev. B **75**, 125328 (2007).
[29] N. C. Giebink and S. R. Forrest, Phys. Rev. B **77**, 235215 (2008).
[30] A. Uddin and C. B. Lee, Phys. Status Solidi C **8**, 80 (2011).
[31] M. Lehnhardt, T. Riedl, T. Rabe, and W. Kowalsky, Org. Electron. **12**, 486 (2011).
[32] A. Uddin, C. B. Lee, and T. G. Andersson, Phys. Status Solidi A **207**, 2334 (2010).
[33] N. Tessler, N. T. Harrison, D. S. Thomas, and R. H. Friend, Appl. Phys. Lett. **73**, 732 (1998).
[34] S. Watanabe, A. Furube, and R. Katoh, J. Phys. Chem. A **110**, 10173 (2006).